Application of Pin-by-pin Fine Mesh Calculation Method to BWR Core Analysis

Kenichi TADA[1], Akio YAMAMOTO, Yasunori KITAMURA, Yoshihiro YAMANE

Nagoya University, Furo-cho, Chikusa-ku, Nagoya, Japan, 464-8603

Abstract

In this paper, a pin-by-pin fine mesh core calculation method, which has been used in PWR, is applied to BWR as a candidate of next-generation core calculation method. Results of pin-by-pin fine mesh core calculation, in which fuel cells are homogenized, are compared with those of heterogeneous transport calculation. By applying the pin-by-pin fine mesh calculation with the SPH correction, multiplication factor and pin-wise fission rate distribution obtained by the heterogeneous calculation is accurately reproduced by the cell-homogenized fine-mesh calculation in BWR multi-assemblies geometry.

KEYWORDS: Pin-by-pin core calculation, BWR, AEGIS, SRAC, SPH method

1. Introduction

The advanced nodal method, which performs homogenization inside an assembly, has been widely used for BWR core analyses at production level calculations and its reliability for current BWR cores has been established through rich experience.

Though UO2 fuel assemblies are mainly loaded to current BWR cores, more advanced fuel assemblies, e.g., high Pu content MOX fuel assemblies, high burnup fuel assemblies with high Gd content fuel rods and an assembly in which Gd fuel rods are located at peripheral region, will be introduced in the future. Such heterogeneous fuel assemblies from the viewpoint of neutronics properties will make precise prediction of core characteristics more difficult, especially local properties such as pin power. Since the advanced nodal method homogenizes fuel assembly, pin power reconstruction for highly heterogeneous fuel assembly would be difficult. Therefore, development of next generation core calculation methods that will overcome the shortcomings of the present method is important.

As an accurate core calculation method, a heterogeneous transport calculation in three-dimensional geometry would be considered. Actually, some aggressive works related to this topic are undergoing. [1] However, the authors think that direct application of the heterogeneous transport calculation in three-dimensional geometry requires considerable computation time that would not suitable for production core calculations. Therefore, in this paper, the pin-by-pin fine mesh core calculation method is considered as a candidate of next-generation core calculation method for BWR. Though heterogeneous structure inside a fuel cell is homogenized, independent mesh is assigned to each fuel cell. Since fuel rods inside an assembly are not homogenized, prediction accuracy of pin power will be higher than that of the current advanced nodal method.

Though pin-by-pin fine mesh core calculation has been applied to PWR and its prediction accuracy has been investigated, it has not been used in BWR core analyses to authors' knowledge. [2] Since structures of

[1] Corresponding author: k-tada@fermi.nucl.nagoya-u.ac.jp

core and fuel assembly are significantly different between PWR and BWR, prediction accuracy and issues of the pin-by-pin core calculation method for BWR core analyses are not clarified so far. Especially, treatments of cruciform control blade, mixed loading of different types of assembly (e.g. 9x9 and 10x10), large water hole, part-length fuel rod and so on in the pin-by-pin fine mesh core calculation were not investigated.

The homogenization error is not negligible when the flux-volume weighted homogenization is simply applied to fuel cell. Therefore, the SPH method [3] is used for the pin-by-pin fine mesh calculation to mitigate the homogenization error.

In this paper, two-dimensional, 2x2 multi-assemblies geometry is analyzed to investigate prediction accuracy of the pin-by-pin fine mesh core calculation method. In particular, results of pin-by-pin fine mesh core calculation, in which fuel cells are homogenized, are compared with those of heterogeneous transport calculation.

2. The SPH Method

The SPH method is a technique that reproduces a result of heterogeneous calculation by that of a homogeneous calculation. [3] Brief description of the SPH method is shown below:

In the traditional flux-volume weighted approach, homogenized cross section of the fuel cell *Cm* ($\overline{\Sigma}_{Cm}$) is given by Eq. (1):

$$\overline{\Sigma}_{Cm} = \sum_{m\in Cm} \Sigma_m \phi_m^{hetero} V_m \Big/ \sum_{m\in Cm} \phi_m^{hetero} V_m \tag{1}$$

where, *Cm* and *m* represent fuel cell and region in the fuel cell, respectively, ϕ_m^{hetero} and V_m are the heterogeneous neutron flux and volume of region *m*, respectively.

Equation (1) is based on the assumption that the Eq. (2) is established.

$$\Sigma_{Cm} \phi^{hom\,o} V_{cm} = \Sigma_{Cm} \sum_{m\in Cm} \phi_m^{hetero} V_m = \sum_{m\in Cm} \Sigma_m \phi_m^{hetero} V_m \tag{2}$$

where, $\phi_{Cm}^{hom\,o}$ and V_{Cm} are the integrated neutron flux and volume of region *Cm*, respectively.

When Eq. (2) has equality, the reaction rates in the homogeneous system are equivalent with those in the heterogeneous system. However, in general, Eq.(2) does not have equality since boundary conditions of fuel cell between heterogeneous and homogeneous systems are not consistent.

In the SPH method, the homogenized cross section $\overline{\Sigma}$ is multiplied by the SPH factor μ in order to preserve the reaction rates:

$$\widetilde{\Sigma}_{Cm} = \mu_{Cm} \overline{\Sigma}_{Cm} \tag{3}$$

where, $\widetilde{\Sigma}$ is cross section which reproduces the result of heterogeneous calculation, $\overline{\Sigma}$ is flux-volume weighted cross section obtained by Eq.(1) and μ_{Cm} is the SPH factor.

The SPH factor is obtained by Eq.(4).

$$\mu_{Cm} = \sum_{m\in Cm} \phi_m^{hetero} V_m \Big/ \phi_{Cm}^{hom\,o} V_{Cm} \tag{4}$$

In actual calculation, the SPH factor in each fuel cell is obtained by the following iteration procedure:

1. First of all, using Eq. (3), the cross sections in first iteration, $\widetilde{\Sigma}^{(1)}$, are generated under the assumption that the SPH factor is unity, i.e., $\mu_{Cm}^{(0)}$=1.
2. Next, calculation using the homogenized cross section of $\widetilde{\Sigma}^{(1)}$ is carried out to obtain the neutron flux in homogeneous system $\phi_{Cm}^{hom\,o}$.
3. The SPH factor is updated using Eq.(4).

4. Using the updated SPH factor, the cross sections in second iteration $\tilde{\Sigma}^{(2)}$ are generated by Eq. (3).
5. Repeat 2-4 until convergence.
6. The above iteration calculation is carried out by Eq. (5) is satisfied.

$$\max\left[\left|\mu_{Cm}^{(n)} - \mu_{Cm}^{(n-1)}\right| \Big/ \mu_{Cm}^{(n)}\right] < \varepsilon, \quad (5)$$

where, ε is a convergence criterion.

3. Calculations

3.1 Calculation flow

In this study, the SPH factor is obtained by the single assembly calculation since multi-assemblies calculation is not usually used in the production calculation. The SPH factor obtained in the single assembly calculation is applied to 2x2 multi-assemblies geometry and homogeneous calculation in the 2x2 multi-assemblies geometry is compared with heterogeneous (reference) 2x2 calculation. Calculation flow is summarized in Fig. 1.

Figure 1: Calculation flow of this study

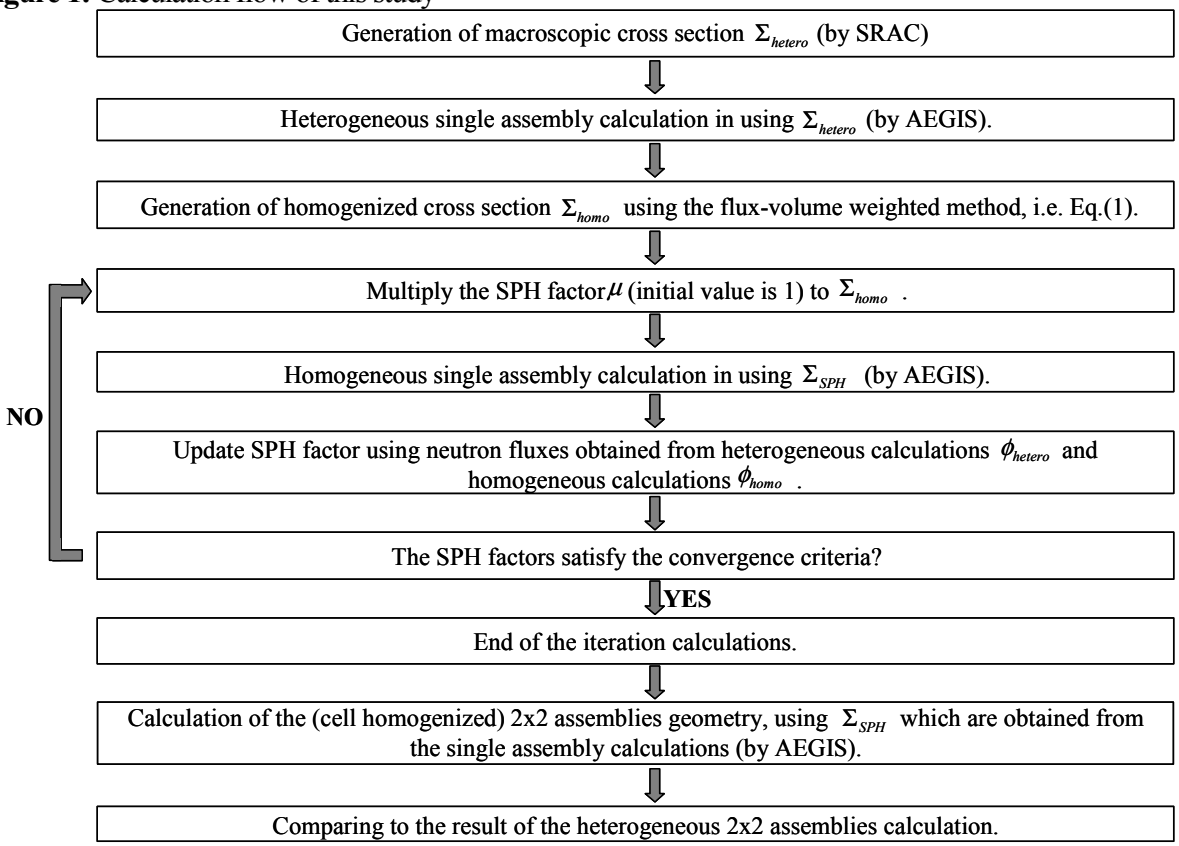

3.2 Calculation codes

In this study, the AEGIS code is used for transport calculations. The AEGIS code is a neutron transport solver based on the method of characteristics (MOC) and being developed by Nuclear Engineering, Ltd. and Nuclear Fuel Industries, Ltd. under cooperation with Nagoya University.[4] Since the AEGIS code can handle the flexible geometric configuration, it can accurately handle the complex BWR assemblies which is

used this study.

The heterogeneous cross sections are generated by the SRAC code. The SRAC code is a multipurpose neutronics calculation code system which contains various calculation routines. [5]

3.3 Calculation geometries and conditions

In this study, two different configurations shown in Fig.8 are analyzed. In the first case (Type-A), two different types of assembly (9x9 and 10x10) are used. Fine mesh boundaries in pin-by-pin calculation are not contiguous at assembly boundary since different types of assembly are used. Furthermore, since two different types of assembly use different fuel materials i.e., UO2 and MOX, the 2x2 assemblies configuration is heterogeneous from the view point of neutronics properties.

The another case, i.e., Type-B, only 9x9 fuel assembly is used, but two different enrichment splittings are assigned. Since the same geometry is used for all assemblies, fine-mesh at assembly boundary is contiguous. Note that control blade is inserted at the center of 2x2 multi-assemblies.

Figure 8: 2x2 multi-assemblies geometry

Type-A

UO_2	UO_2
MOX	MOX

Type-B

Low	Low
High	High

Part of the assembly specifications is taken from the benchmark suite for next-generation fuels of LWR.[6] In Type-A, two different BWR assemblies given in the benchmark suite shown in Figs. 2 and 3 are used in the calculation. The UO2 and MOX fuel assemblies are based on GE11 (9x9) and Atrium 10 (10x10), respectively. Figures 4 and 5 show cell homogeneous assemblies used for pin-by-pin fine mesh calculations.

In Type-B, geometry of the UO2 fuel assembly is used. Figures 6 and 7 show the enrichment splitting of the high and low enrichment assemblies and Table 1 show the composition of the fuel pins.

Figure 2: Heterogeneous UO_2 assembly (UO_2)

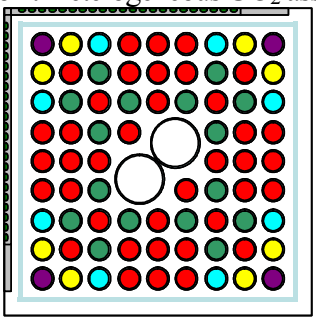

Figure 3: Heterogeneous MOX assembly (MOX)

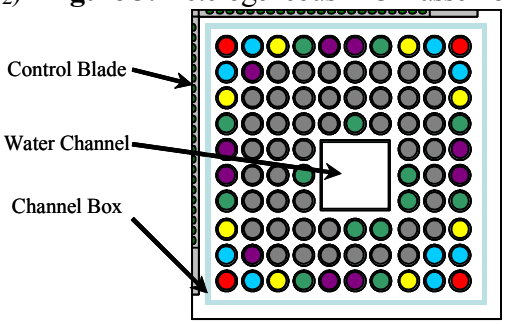

Figure 4: Homogeneous UO_2 assembly

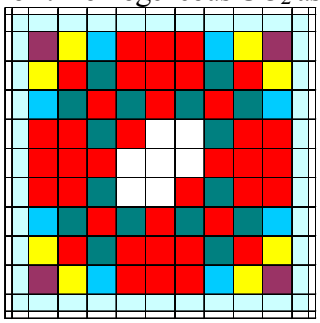

Figure 5: Homogeneous MOX assembly

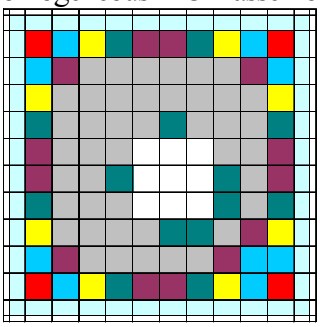

Figure6: Specification of the high enrichment UO2 assembly (High)

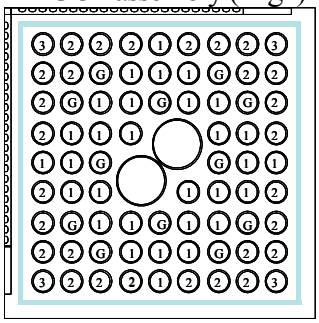

Figure7: Specification of the low enrichment UO2 assembly (Low)

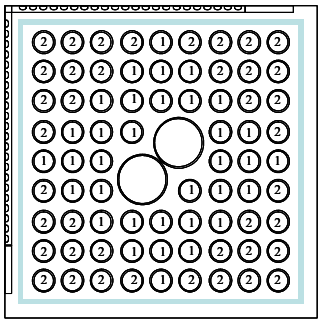

Table 1: Composition of Each Fuel Pin

	Highly enriched UO_2 assembly				Lowly enrichment UO_2 assembly	
	Type-1	Type-2	Type-3	Type-G	Type-1	Type-2
Number of rods	30	28	4	12	34	74
UO_2 density (g/cc)	10.5	10.5	10.5	10.4	10.5	10.5
^{235}U enrichment (wt%)	4.5	3.5	2.0	4.5	1.2	0.7
Gd_2O_3 concentration (wt%)				4.0		
Atomic number density (#/barn/cm)						
^{235}U	1.0657E-03	8.2889E-04	4.7365E-04	1.0133E-03	2.8419E-04	1.6578E-04
^{238}U	2.2366E-02	2.2600E-02	2.2951E-02	2.1266E-02	2.3138E-02	2.3256E-02
^{16}O	4.6863E-02	4.6857E-02	4.6849E-02	4.6633E-02	4.6845E-02	4.6843E-02
^{154}Gd				3.0192E-05		
^{155}Gd				2.0497E-04		
^{156}Gd				2.8350E-04		
^{157}Gd				2.1675E-04		
^{158}Gd				3.4402E-02		
^{160}Gd				3.0275E-04		

The energy group structure used in this study is shown in Table 2. In this study, 8 energy groups are used throughout the calculations. The relative convergence criteria of the SPH factor was set to be 1.0×10^{-3}.

In AEGIS, the relative convergence criteria for neutron flux and k-effective were set to be 1.0×10^{-4} and 1.0×10^{-5}, respectively. To decrease the mesh discretization error, heterogeneous and homogeneous cells are azimuthally divided into 8 regions. The ray trace method is the material region macroband (track spacing is less than 0.1cm).[7] Numbers of azimuthal and polar angle are 96 and 2 (TY optimum), respectively. [8]

Reflective boundary condition is used both for the single assembly and 2x2 assemblies.

Table 2: The energy group structure that is used calculation.

Upper limits(eV)	1.00E+07	8.21E+05	5.53E+03	3.93E+00	9.93E-01	6.02E-01	1.37E-01	5.45E-02
Lower limits(eV)	8.21E+05	5.53E+03	3.93E+00	9.93E-01	6.02E-01	1.37E-01	5.45E-02	1.00E-05

3.4 Calculation results

3.4.1 Calculation result of Type-A

Table 3 shows that reference k-infinity in cell heterogeneous 2x2 assemblies geometry is well reproduced by the fine mesh calculation with the SPH method. The maximum (MAX diff.) and root mean square (RMS) differences of pin-wise fission rate distribution between heterogeneous (reference) and homogeneous (fine-mesh) calculations are shown in Figs. 9~12. Figures 9~12 indicate that though significant errors are found in the homogeneous calculation without the SPH factor, the errors are significantly reduced in the homogeneous calculation with the SPH factor. Figures 9~12 also indicate that though the present 2x2 assemblies configuration has non-contiguous mesh at assembly boundary, pin-by-pin fine mesh calculation with the SPH factor works well.

In this study, the SPH factor is obtained by the single assembly calculations. Therefore, even if the SPH factor is applied, slight difference is observed in the assembly peripheral region in which boundary condition in 2x2 assemblies calculation is considerably different from that of the single assembly calculation.

3.4.2 Calculation result of Type-B

As Type-A, Table 4 shows that reference k-infinity in cell heterogeneous 2x2 assembly geometry is well reproduced by the fine mesh calculation with the SPH method. The maximum (MAX diff.) and root mean square (RMS) difference of pin-wise fission rate distribution between heterogeneous (reference) and homogeneous (fine-mesh) calculations are shown in Figs. 13~16.

The SPH method has sufficient accuracy to reproduce the reference result as in the case of Type-A. The region in which different assemblies are adjacent also shows larger error. Comparing Type-A and Type-B, though the largest difference is approximately equivalent, the RMS of Type-B is slightly larger than that of Type-A.

Consequently, by applying the pin-by-pin fine mesh calculation with the SPH correction, multiplication factor and pin-wise fission rate distribution obtained by the heterogeneous calculation is accurately reproduced by the cell-homogenized fine-mesh transport calculation in BWR multi-assemblies geometry.

Table 3: Comparison of k-infinity in 2x2 multi-assemblies geometry.

	Reference	No-SPH	(No-SPH - Ref)/Ref	SPH	(SPH - Ref)/Ref
k_{inf}	1.0818	1.0684	-1.23%	1.0822	0.04%

Table 4: Comparison of k-infinity in 2x2 multi-assemblies geometry.

	Reference	No-SPH	(No-SPH - Ref)/Ref	SPH	(SPH - Ref)/Ref
k_{inf}	0.7645	0.7395	-3.27%	0.7647	0.02%

Figure 9: The discrepancy of pin-wise fission rate distribution between heterogeneous (reference) and homogeneous (fine-mesh) calculations without the SPH factor. (Upper left, UO2)

1.746	1.770	1.776	1.960	1.887	1.826	1.519	1.366	1.206
1.705	1.720	1.715	1.908	1.840	1.776	1.463	1.319	1.162
-2.34%	-2.83%	-3.42%	-2.64%	-2.50%	-2.71%	-3.64%	-3.44%	-3.59%
1.774	1.777	0.494	1.366	1.419	1.287	0.433	1.290	1.024
1.725	1.709	0.495	1.309	1.370	1.233	0.433	1.237	0.989
-2.76%	-3.80%	0.19%	-4.19%	-3.43%	-4.16%	0.03%	-4.12%	-3.41%
1.788	0.496	1.131	0.456	1.398	0.439	0.995	0.381	0.863
1.730	0.497	1.063	0.455	1.323	0.439	0.929	0.381	0.839
-3.24%	0.31%	-6.00%	-0.13%	-5.37%	-0.11%	-6.67%	0.12%	-2.73%
1.983	1.379	0.458	1.554			0.405	0.910	0.891
1.937	1.326	0.458	1.482			0.405	0.879	0.879
-2.30%	-3.90%	0.03%	-4.63%			0.02%	-3.43%	-1.33%
1.920	1.440	1.412				1.185	0.941	0.843
1.882	1.398	1.340				1.123	0.914	0.836
-1.94%	-2.97%	-5.07%				-5.22%	-2.90%	-0.87%
1.867	1.314	0.448			1.403	0.374	0.836	0.800
1.831	1.268	0.450			1.339	0.375	0.810	0.794
-1.92%	-3.49%	0.45%			-4.56%	0.36%	-3.17%	-0.84%
1.556	0.447	1.020	0.414	1.200	0.378	0.797	0.327	0.651
1.516	0.452	0.959	0.417	1.142	0.380	0.756	0.331	0.641
-2.57%	1.02%	-5.90%	0.66%	-4.86%	0.60%	-5.07%	1.00%	-1.43%
1.391	1.320	0.395	0.935	0.961	0.850	0.331	0.789	0.586
1.363	1.282	0.400	0.910	0.939	0.826	0.335	0.772	0.580
-2.06%	-2.85%	1.26%	-2.68%	-2.34%	-2.78%	1.26%	-2.11%	-0.91%
1.205	1.035	0.884	0.916	0.864	0.816	0.658	0.588	0.506
1.182	1.016	0.870	0.911	0.862	0.813	0.651	0.583	0.499
-1.90%	-1.87%	-1.62%	-0.56%	-0.30%	-0.45%	-1.15%	-0.83%	-1.37%

cell average fission rate

reference
No-SPH
difference

RMS = 2.93%

MAXdiff. = 6.67%

Figure 10: The discrepancy of pin-wise fission rate distribution between heterogeneous (reference) and homogeneous (fine-mesh) calculations with the SPH factor. (Upper left, UO2)

1.746	1.770	1.776	1.960	1.887	1.826	1.519	1.366	1.206
1.745	1.769	1.775	1.959	1.886	1.825	1.519	1.366	1.206
-0.05%	-0.04%	-0.04%	-0.04%	-0.04%	-0.02%	-0.01%	0.00%	0.02%
1.774	1.777	0.494	1.366	1.419	1.287	0.433	1.290	1.024
1.774	1.776	0.493	1.365	1.418	1.287	0.433	1.290	1.024
-0.05%	-0.04%	-0.05%	-0.03%	-0.04%	-0.02%	-0.04%	0.00%	0.01%
1.788	0.496	1.131	0.456	1.398	0.439	0.995	0.381	0.863
1.787	0.496	1.131	0.455	1.397	0.439	0.995	0.380	0.863
-0.05%	-0.06%	-0.04%	-0.07%	-0.06%	-0.06%	-0.03%	-0.04%	0.01%
1.983	1.379	0.458	1.554			0.405	0.910	0.891
1.982	1.379	0.458	1.553			0.405	0.910	0.891
-0.04%	-0.05%	-0.07%	-0.07%			-0.05%	-0.04%	-0.01%
1.920	1.440	1.412				1.185	0.941	0.843
1.919	1.440	1.411				1.185	0.941	0.843
-0.03%	-0.05%	-0.06%				-0.03%	-0.03%	-0.03%
1.867	1.314	0.448			1.403	0.374	0.836	0.800
1.866	1.314	0.448			1.403	0.374	0.836	0.800
-0.02%	-0.04%	-0.05%			-0.01%	-0.02%	-0.01%	-0.02%
1.556	0.447	1.020	0.414	1.200	0.378	0.797	0.327	0.651
1.556	0.447	1.019	0.414	1.199	0.377	0.797	0.327	0.651
0.01%	-0.05%	-0.07%	-0.07%	-0.03%	-0.03%	0.01%	0.01%	0.04%
1.391	1.320	0.395	0.935	0.961	0.850	0.331	0.789	0.586
1.392	1.320	0.395	0.933	0.961	0.850	0.331	0.790	0.587
0.01%	-0.03%	-0.10%	-0.16%	-0.08%	0.02%	0.04%	0.19%	0.26%
1.205	1.035	0.884	0.916	0.864	0.816	0.658	0.588	0.506
1.206	1.035	0.882	0.914	0.864	0.818	0.662	0.591	0.509
0.08%	-0.01%	-0.22%	-0.23%	-0.04%	0.24%	0.52%	0.58%	0.71%

cell average fission rate

reference
SPH
difference

RMS = 0.14%

MAXdiff. = 0.71%

Figure 11: The discrepancy of pin-wise fission rate distribution between heterogeneous (reference) and homogeneous (fine-mesh) calculations without the SPH factor. (Lower left, MOX)

1.230	0.967	0.853	0.236	0.700	0.674	0.216	0.626	0.526	0.493
1.215	0.968	0.876	0.242	0.722	0.696	0.221	0.645	0.537	0.492
-1.24%	0.05%	2.73%	2.46%	3.11%	3.23%	2.38%	2.96%	1.96%	-0.36%
1.246	1.097	0.948	0.844	0.804	0.778	0.757	0.758	0.693	0.527
1.241	1.124	0.982	0.872	0.831	0.802	0.781	0.783	0.713	0.537
-0.39%	2.42%	3.55%	3.28%	3.26%	3.10%	3.07%	3.28%	2.83%	1.90%
1.438	1.117	0.942	0.922	0.925	0.871	0.808	0.763	0.764	0.632
1.443	1.156	0.975	0.954	0.951	0.899	0.832	0.788	0.790	0.652
0.35%	3.48%	3.53%	3.43%	2.83%	3.17%	3.09%	3.38%	3.45%	3.18%
0.345	1.111	1.113	1.386	0.316	1.334	0.996	0.814	0.770	0.222
0.352	1.148	1.134	1.407	0.322	1.350	1.009	0.841	0.796	0.229
2.03%	3.30%	1.97%	1.46%	1.99%	1.19%	1.30%	3.27%	3.42%	3.11%
1.502	1.172	1.465				1.341	0.884	0.797	0.690
1.513	1.216	1.493				1.358	0.915	0.825	0.716
0.71%	3.74%	1.90%				1.32%	3.48%	3.59%	3.66%
1.549	1.246	0.347				0.320	0.944	0.828	0.721
1.564	1.290	0.356				0.327	0.975	0.860	0.747
0.95%	3.57%	2.51%				2.27%	3.28%	3.87%	3.65%
0.373	1.293	0.345				1.405	0.945	0.873	0.247
0.382	1.342	0.354				1.431	0.983	0.908	0.256
2.62%	3.82%	2.69%				1.82%	4.02%	4.06%	3.56%
1.690	1.232	1.353	0.346	0.350	1.482	1.135	0.970	0.980	0.871
1.721	1.278	1.387	0.355	0.359	1.515	1.163	1.011	1.024	0.905
1.86%	3.68%	2.56%	2.77%	2.72%	2.21%	2.49%	4.27%	4.54%	3.80%
1.566	1.056	1.236	1.302	1.261	1.194	1.139	1.151	1.124	0.968
1.596	1.083	1.283	1.354	1.309	1.244	1.184	1.201	1.165	0.984
1.92%	2.59%	3.74%	3.99%	3.86%	4.18%	3.94%	4.39%	3.68%	1.67%
1.638	1.570	1.699	0.376	1.573	1.533	0.355	1.475	1.266	1.217
1.665	1.600	1.732	0.387	1.593	1.552	0.365	1.495	1.279	1.223
1.66%	1.96%	1.95%	2.81%	1.30%	1.23%	2.76%	1.39%	0.98%	0.47%

cell average fission rate

reference
No-SPH
difference

RMS = 2.87%
MAXdiff. = 4.54%

Figure 12: The discrepancy of pin-wise fission rate distribution between heterogeneous (reference) and homogeneous (fine-mesh) calculations with the SPH factor. (Lower left, MOX)

1.230	0.967	0.853	0.236	0.700	0.674	0.216	0.626	0.526	0.493
1.228	0.965	0.854	0.236	0.700	0.672	0.215	0.622	0.523	0.489
-0.20%	-0.18%	0.13%	0.14%	-0.06%	-0.25%	-0.19%	-0.69%	-0.67%	-0.93%
1.246	1.097	0.948	0.844	0.804	0.778	0.757	0.758	0.693	0.527
1.245	1.097	0.949	0.846	0.805	0.778	0.757	0.757	0.692	0.525
-0.08%	-0.05%	0.09%	0.16%	0.11%	0.02%	-0.06%	-0.13%	-0.21%	-0.38%
1.438	1.117	0.942	0.922	0.925	0.871	0.808	0.763	0.764	0.632
1.437	1.117	0.943	0.923	0.926	0.872	0.807	0.762	0.763	0.631
-0.05%	0.03%	0.08%	0.08%	0.04%	0.02%	-0.01%	-0.01%	-0.04%	-0.11%
0.345	1.111	1.113	1.386	0.316	1.334	0.996	0.814	0.770	0.222
0.345	1.111	1.113	1.387	0.316	1.334	0.995	0.814	0.770	0.222
0.04%	0.05%	0.02%	0.01%	0.03%	-0.02%	-0.03%	-0.01%	0.00%	0.02%
1.502	1.172	1.465				1.341	0.884	0.797	0.690
1.502	1.173	1.466				1.340	0.884	0.797	0.690
0.01%	0.03%	0.02%				-0.01%	0.00%	0.00%	-0.01%
1.549	1.246	0.347				0.320	0.944	0.828	0.721
1.550	1.246	0.347				0.320	0.944	0.828	0.721
0.04%	0.04%	0.04%				0.03%	0.01%	0.02%	0.02%
0.373	1.293	0.345				1.405	0.945	0.873	0.247
0.373	1.293	0.345				1.405	0.946	0.873	0.247
0.07%	0.05%	0.05%				0.04%	0.03%	0.02%	0.05%
1.690	1.232	1.353	0.346	0.350	1.482	1.135	0.970	0.980	0.871
1.691	1.233	1.353	0.346	0.350	1.483	1.135	0.970	0.980	0.872
0.07%	0.05%	0.06%	0.05%	0.05%	0.05%	0.05%	0.03%	0.02%	0.03%
1.566	1.056	1.236	1.302	1.261	1.194	1.139	1.151	1.124	0.968
1.567	1.057	1.237	1.302	1.261	1.194	1.139	1.151	1.124	0.968
0.07%	0.07%	0.04%	0.04%	0.03%	0.03%	0.03%	0.03%	0.03%	0.04%
1.638	1.570	1.699	0.376	1.573	1.533	0.355	1.475	1.266	1.217
1.639	1.571	1.700	0.377	1.573	1.534	0.355	1.475	1.267	1.218
0.07%	0.06%	0.04%	0.05%	0.03%	0.03%	0.04%	0.03%	0.04%	0.05%

cell average fission rate

reference
SPH
difference

RMS = 0.16%
MAXdiff. = 0.93%

Figure 13: The discrepancy of pin-wise fission rate distribution between heterogeneous (reference) and homogeneous (fine-mesh) calculations without the SPH factor. (Upper left, Low enrichment)

1.015	0.937	0.879	0.827	1.255	0.749	0.716	0.678	0.645
1.063	0.980	0.918	0.864	1.313	0.780	0.744	0.701	0.663
4.74%	4.59%	4.51%	4.39%	4.65%	4.11%	3.91%	3.47%	2.70%
0.941	0.857	0.798	1.199	1.137	1.082	0.637	0.585	0.515
0.983	0.894	0.832	1.254	1.188	1.129	0.662	0.607	0.531
4.51%	4.40%	4.34%	4.60%	4.47%	4.35%	3.92%	3.62%	3.10%
0.889	0.803	1.198	1.156	1.135	1.064	0.944	0.520	0.427
0.927	0.837	1.252	1.208	1.186	1.111	0.986	0.540	0.443
4.31%	4.21%	4.55%	4.50%	4.46%	4.44%	4.39%	3.80%	3.81%
0.844	1.218	1.166	1.204			0.922	0.753	0.378
0.878	1.270	1.216	1.254			0.960	0.783	0.393
4.02%	4.30%	4.32%	4.21%			4.15%	4.03%	3.88%
1.294	1.167	1.157				0.876	0.699	0.542
1.347	1.213	1.204				0.910	0.726	0.564
4.06%	3.98%	4.09%				3.85%	3.84%	4.08%
0.782	1.123	1.096			0.960	0.787	0.650	0.329
0.808	1.164	1.138			0.994	0.816	0.674	0.340
3.27%	3.61%	3.83%			3.53%	3.63%	3.64%	3.46%
0.754	0.669	0.984	0.953	0.896	0.796	0.699	0.385	0.312
0.776	0.689	1.019	0.986	0.926	0.823	0.722	0.397	0.322
2.79%	2.86%	3.47%	3.44%	3.35%	3.36%	3.38%	2.98%	2.99%
0.718	0.620	0.549	0.788	0.724	0.666	0.390	0.350	0.295
0.733	0.634	0.563	0.811	0.745	0.686	0.400	0.359	0.302
2.04%	2.21%	2.48%	2.90%	2.93%	2.99%	2.62%	2.46%	2.39%
0.679	0.546	0.455	0.401	0.568	0.341	0.320	0.299	0.276
0.685	0.553	0.464	0.410	0.582	0.349	0.327	0.304	0.278
0.96%	1.27%	1.94%	2.15%	2.58%	2.24%	2.09%	1.88%	0.99%

cell average fission rate

reference
No-SPH
difference

RMS = 3.61%

MAXdiff. = 4.74%

Figure 14: The discrepancy of pin-wise fission rate distribution between heterogeneous (reference) and homogeneous (fine-mesh) calculations with the SPH factor. (Upper left, Low enrichment)

1.015	0.937	0.879	0.827	1.255	0.749	0.716	0.678	0.645
1.013	0.935	0.877	0.826	1.253	0.748	0.715	0.677	0.645
-0.15%	-0.15%	-0.15%	-0.15%	-0.14%	-0.14%	-0.13%	-0.11%	-0.08%
0.941	0.857	0.798	1.199	1.137	1.082	0.637	0.585	0.515
0.939	0.855	0.796	1.197	1.135	1.080	0.636	0.585	0.514
-0.15%	-0.15%	-0.15%	-0.15%	-0.16%	-0.15%	-0.14%	-0.11%	-0.07%
0.889	0.803	1.198	1.156	1.135	1.064	0.944	0.520	0.427
0.888	0.802	1.196	1.154	1.133	1.062	0.943	0.520	0.426
-0.14%	-0.15%	-0.16%	-0.16%	-0.17%	-0.15%	-0.14%	-0.12%	-0.08%
0.844	1.218	1.166	1.204			0.922	0.753	0.378
0.843	1.216	1.164	1.202			0.921	0.752	0.378
-0.14%	-0.16%	-0.17%	-0.17%			-0.16%	-0.14%	-0.11%
1.294	1.167	1.157				0.876	0.699	0.542
1.293	1.165	1.155				0.875	0.698	0.541
-0.14%	-0.16%	-0.19%				-0.18%	-0.17%	-0.14%
0.782	1.123	1.096			0.960	0.787	0.650	0.329
0.781	1.121	1.094			0.958	0.785	0.649	0.328
-0.14%	-0.19%	-0.22%			-0.22%	-0.22%	-0.21%	-0.19%
0.754	0.669	0.984	0.953	0.896	0.796	0.699	0.385	0.312
0.753	0.668	0.981	0.950	0.893	0.794	0.696	0.384	0.312
-0.14%	-0.24%	-0.31%	-0.33%	-0.34%	-0.33%	-0.31%	-0.27%	-0.20%
0.718	0.620	0.549	0.788	0.724	0.666	0.390	0.350	0.295
0.717	0.618	0.546	0.783	0.720	0.662	0.388	0.349	0.295
-0.12%	-0.33%	-0.53%	-0.63%	-0.64%	-0.59%	-0.49%	-0.34%	-0.14%
0.679	0.546	0.455	0.401	0.568	0.341	0.320	0.299	0.276
0.678	0.543	0.450	0.396	0.560	0.337	0.317	0.297	0.276
-0.05%	-0.57%	-1.09%	-1.31%	-1.38%	-1.15%	-0.88%	-0.54%	0.05%

cell average fission rate

reference
SPH
difference

RMS = 0.39%

MAXdiff. = 1.38%

Figure 15: The discrepancy of pin-wise fission rate distribution between heterogeneous (reference) and homogeneous (fine-mesh) calculations without the SPH factor. (Lower left, High enrichment)

1.255	1.343	0.950	0.833	0.936	0.723	0.672	0.696	0.478
1.238	1.334	0.947	0.836	0.949	0.726	0.671	0.698	0.473
-1.40%	-0.69%	-0.35%	0.41%	1.35%	0.47%	-0.17%	0.34%	-0.97%
1.798	1.231	0.122	1.116	1.042	0.980	0.102	0.693	0.702
1.777	1.195	0.124	1.094	1.030	0.963	0.104	0.677	0.699
-1.17%	-2.91%	1.66%	-1.95%	-1.18%	-1.81%	1.52%	-2.31%	-0.33%
1.731	0.139	1.337	1.443	0.124	1.199	1.017	0.105	0.688
1.695	0.141	1.293	1.395	0.125	1.158	0.983	0.106	0.680
-2.10%	1.43%	-3.34%	-3.37%	1.19%	-3.41%	-3.31%	1.18%	-1.28%
1.816	1.650	1.629			1.685	1.214	1.008	0.751
1.783	1.602	1.571			1.630	1.170	0.983	0.743
-1.83%	-2.90%	-3.55%			-3.24%	-3.61%	-2.47%	-0.97%
2.313	1.732	0.150				0.128	1.085	0.984
2.287	1.693	0.151				0.129	1.063	0.980
-1.13%	-2.25%	0.83%				0.72%	-2.07%	-0.37%
1.996	1.785	1.665	1.986			1.492	1.173	0.883
1.955	1.731	1.603	1.922			1.435	1.138	0.870
-2.06%	-3.00%	-3.75%	-3.20%			-3.85%	-2.95%	-1.49%
2.120	0.167	1.593	1.679	0.153	1.678	1.396	0.131	1.009
2.066	0.168	1.531	1.615	0.154	1.612	1.341	0.132	0.985
-2.55%	0.86%	-3.90%	-3.86%	0.56%	-3.93%	-3.98%	0.53%	-2.37%
2.478	1.815	0.168	1.815	1.781	1.715	0.148	1.304	1.411
2.437	1.747	0.169	1.757	1.734	1.656	0.148	1.250	1.375
-1.65%	-3.75%	0.78%	-3.22%	-2.63%	-3.45%	0.59%	-4.19%	-2.54%
1.916	2.489	2.145	2.038	2.387	1.896	1.825	1.898	1.305
1.884	2.446	2.087	1.991	2.349	1.849	1.770	1.851	1.265
-1.64%	-1.71%	-2.70%	-2.33%	-1.58%	-2.47%	-3.02%	-2.47%	-3.07%

cell average fission rate

reference	
No-SPH	
difference	
RMS =	2.38%
MAXdiff. =	4.19%

Figure 16: The discrepancy of pin-wise fission rate distribution between heterogeneous (reference) and homogeneous (fine-mesh) calculations with the SPH factor. (Lower left, High enrichment)

1.255	1.343	0.950	0.833	0.936	0.723	0.672	0.696	0.478
1.254	1.348	0.958	0.840	0.942	0.726	0.673	0.695	0.475
-0.14%	0.36%	0.85%	0.82%	0.65%	0.41%	0.12%	-0.08%	-0.58%
1.798	1.231	0.122	1.116	1.042	0.980	0.102	0.693	0.702
1.797	1.232	0.122	1.119	1.045	0.982	0.103	0.693	0.700
-0.06%	0.13%	0.21%	0.31%	0.32%	0.20%	0.14%	-0.02%	-0.25%
1.731	0.139	1.337	1.443	0.124	1.199	1.017	0.105	0.688
1.731	0.139	1.339	1.445	0.124	1.200	1.018	0.105	0.688
0.01%	0.14%	0.13%	0.12%	0.18%	0.10%	0.09%	0.14%	-0.03%
1.816	1.650	1.629			1.685	1.214	1.008	0.751
1.817	1.651	1.631			1.687	1.215	1.009	0.751
0.06%	0.10%	0.12%			0.10%	0.12%	0.09%	0.07%
2.313	1.732	0.150				0.128	1.085	0.984
2.315	1.734	0.150				0.128	1.087	0.985
0.10%	0.12%	0.17%				0.17%	0.12%	0.10%
1.996	1.785	1.665	1.986			1.492	1.173	0.883
1.999	1.787	1.668	1.989			1.494	1.174	0.884
0.13%	0.14%	0.14%	0.15%			0.13%	0.14%	0.11%
2.120	0.167	1.593	1.679	0.153	1.678	1.396	0.131	1.009
2.123	0.167	1.596	1.682	0.153	1.681	1.398	0.132	1.011
0.14%	0.18%	0.16%	0.15%	0.19%	0.16%	0.15%	0.20%	0.12%
2.478	1.815	0.168	1.815	1.781	1.715	0.148	1.304	1.411
2.482	1.817	0.168	1.818	1.783	1.718	0.148	1.306	1.413
0.16%	0.14%	0.20%	0.14%	0.13%	0.15%	0.20%	0.13%	0.13%
1.916	2.489	2.145	2.038	2.387	1.896	1.825	1.898	1.305
1.919	2.493	2.148	2.041	2.390	1.898	1.828	1.901	1.307
0.16%	0.15%	0.15%	0.15%	0.15%	0.15%	0.14%	0.15%	0.16%

cell average fission rate

reference	
SPH	
difference	
RMS =	0.23%
MAXdiff. =	0.85%

4. Conclusions

In this study, the pin-by-pin fine mesh core calculation method is validated as a candidate of next-generation core calculation method for BWR. To investigate prediction accuracy of the pin-by-pin fine mesh core calculation method, 2x2 multi-assemblies geometry in two dimension is analyzed with the pin-by-pin fine mesh geometry and transport calculation. The SPH method is used for the pin-by-pin fine mesh calculation to mitigate the homogenization error.

The SPH method is obtained by the single assembly calculation. The SPH factor obtained in the single assembly transport calculation is applied to 2x2 multi-assemblies geometry and the fine mesh homogeneous transport calculation in the 2x2 multi-assemblies geometry is compared with heterogeneous transport calculation.

In this study, two different cases are analyzed. The first case (Type-A), two different types of assembly (9x9 and 10x10) are used. Furthermore, two different types of assembly use different fuel materials, i.e., UO2 and MOX. The another case, i.e., Type-B, utilizes the same assembly geometry but two different splittings are used.

By applying the pin-by-pin fine mesh calculation with the SPH correction, multiplication factor and pin-wise fission rate distribution obtained by the heterogeneous calculation is accurately reproduced by the cell-homogenized fine-mesh transport calculation. The present results suggest that application of the pin-by-pin fine-mesh calculation for BWR core analyses will be promising.

Reference

1) H. G. Joo, et al., "Methods and Performance of a Three-Dimensional Whole Core Transport Code DeCART," Proc. PHYSOR2004, Chicago, IL, April 25-29, 2004, on CD-ROM, American Nuclear Society, Lagrange Park, IL. (2004).
2) M. Tatsumi and A. Yamamoto, "Advanced PWR Core Calculation Based on Multi-group Nodal-transport Method in Three-dimensional Pin-by-Pin Geometry," J. Nucl Sci. Tech., **40**, 376 (2003).
3) A. Hebert, "A Consistent Technique for the Pin-by-Pin Homogenization of a Pressurized Water Reactor Assembly," Nucl. Sci. Eng., **113**, 227 (1993).
4) N. Sugimura, T. Ushio, M. Mori and A. Yamamoto, et al., "Development of Advanced Neutronics Design System of Next Generation, AEGIS," Proc. International topical Meeting on Mathematics and Computation, Supercomputing, Reactor Physics and Nuclear and Biological Applications (M&C2005), Avignon, France, Sept. 12-15, (2005). [CD-ROM]
5) K. Tsuchihashi, et al., Revised SRAC Code System, JAERI 1302, Japan Atomic Energy Research Institute, (1986).
6) A. Yamamoto, T. Ikehara and T. Ito et al., "Benchmark Problem Suite for Reactor Physics Study of LWR Next Generation Fuels," J. Nucl Sci. Tech., **39**, 900 (2002).
7) A. Yamamoto, M. Tabuchi and N. Sugimura et al. "Non-equidistant Ray Tracing for the Method of Characteristics," Proc. International topical Meeting on Mathematics and Computation, Supercomputing, Reactor Physics and Nuclear and Biological Applications (M&C2005), Avignon, France, Sept. 12-15, (2005).[CD-ROM]
8) M. Tabuchi, A. Yamamoto and T. Endo, et al., "Yet Another Optimum Polar Angle Quadrature Set for the Method of Characteristics," Trans. Am. Nucl. Soc., **93**, 506 (2005).